

Measurements of $H(z)$ and $D_A(z)$ from the Two-Dimensional Two-Point Correlation Function of Sloan Digital Sky Survey Luminous Red Galaxies

Chia-Hsun Chuang^{*} and Yun Wang

Homer L. Dodge Department of Physics & Astronomy, Univ. of Oklahoma, 440 W Brooks St., Norman, OK 73019, U.S.A.

16 February 2022

ABSTRACT

We present a method for measuring the Hubble parameter, $H(z)$, and angular diameter distance, $D_A(z)$, from the two-dimensional two-point correlation function, and validate it using LasDamas mock galaxy catalogs. Applying our method to the sample of luminous red galaxies (LRGs) from the Sloan Digital Sky Survey (SDSS) Data Release 7 (DR7), we measure $H(z = 0.35) \equiv H(0.35) = 82.1^{+4.8}_{-4.9} \text{ km s}^{-1} \text{ Mpc}^{-1}$, $D_A(z = 0.35) \equiv D_A(0.35) = 1048^{+60}_{-58} \text{ Mpc}$ without assuming a dark energy model or a flat Universe. We find that the derived measurements of $H(0.35)r_s(z_d)/c$ and $D_A(0.35)/r_s(z_d)$ (where $r_s(z_d)$ is the sound horizon at the drag epoch) are nearly uncorrelated, have tighter constraints and are more robust with respect to possible systematic effects. Our galaxy clustering measurements of $\{H(0.35)r_s(z_d)/c, D_A(0.35)/r_s(z_d)\} = \{0.0434 \pm 0.0018, 6.60 \pm 0.26\}$ (with the correlation coefficient $r = 0.0604$) can be used to combine with cosmic microwave background and any other cosmological data sets to constrain dark energy. Our results represent the first measurements of $H(z)$ and $D_A(z)$ (or $H(z)r_s(z_d)/c$ and $D_A(0.35)/r_s(z_d)$) from galaxy clustering data. Our work has significant implications for future surveys in establishing the feasibility of measuring both $H(z)$ and $D_A(z)$ from galaxy clustering data.

Key words: cosmology; observations, distance scale, large-scale structure of Universe

1 INTRODUCTION

The cosmic large-scale structure from galaxy redshift surveys provides a powerful probe of dark energy and the cosmological model that is highly complementary to the cosmic microwave background (CMB) (Bennett et al. 2003), supernovae (SNe) (Riess et al. 1998; Perlmutter et al. 1999), and weak lensing (Wittman et al. 2000; Bacon, Refregier, & Ellis 2000; Kaiser, Wilson, & Luppino 2000; van Waerbeke et al. 2000). The scope of galaxy redshift surveys has dramatically increased in the last decade. The PSCz surveyed $\sim 15,000$ galaxies using the Infrared Astronomical Satellite (IRAS) (Saunders et al. 2000), the 2dF Galaxy Redshift Survey (2dFGRS) obtained 221,414 galaxy redshifts (Colless et al. 2001, 2003), and the Sloan Digital Sky Survey (SDSS) has collected 930,000 galaxy spectra in the Seventh Data Release (DR7) (Abazajian et al. 2009). The ongoing galaxy surveys will probe the Universe at higher redshifts; WiggleZ is surveying 240,000 emission-line galaxies at $0.5 < z < 1$ over 1000 square degrees (Blake et al. 2009), and BOSS is surveying 1.5 million luminous red galaxies (LRGs) at

$0.1 < z < 0.7$ over 10,000 square degrees (Eisenstein et al. 2011). The planned space mission Euclid will survey over 60 million emission-line galaxies at $0.5 < z < 2$ over 20,000 square degrees (Cimatti et al. 2009; Wang et al. 2010).

Large-scale structure data from galaxy surveys can be analyzed using either the power spectrum or the correlation function. Although these two methods are simple Fourier transforms of one another, the analysis processes are quite different and the results cannot be converted using Fourier transform directly because of the finite size of the survey volume. The SDSS data have been analyzed using both the power spectrum method (see, e.g., Tegmark et al. 2004; Hutsi 2005; Padmanabhan et al. 2007; Blake et al. 2007; Percival et al. 2007, 2010; Reid et al. 2009), and the correlation function method (see, e.g., Eisenstein et al. 2005; Okumura et al. 2008; Cabre & Gaztanaga 2008; Martinez et al. 2009; Sanchez et al. 2009; Kazin et al. 2010a; Chuang, Wang, & Hemantha 2012). While previous work has focused on the spherically averaged two-point correlation function (2PCF), or the radial projection of the two-dimensional two point correlation function (2D 2PCF), we measure and analyze the full 2D 2PCF of SDSS LRGs in this study.

^{*} E-mail: chuang@nhn.ou.edu

The power of galaxy clustering as a dark energy probe lies in the fact that the Hubble parameter, $H(z)$, and the angular diameter distance, $D_A(z)$, can in principle be extracted simultaneously from data through the measurement of the baryon acoustic oscillation (BAO) scale in the radial and transverse directions (Blake & Glazebrook 2003; Seo & Eisenstein 2003; Wang 2006). This has not been achieved in the previous work in the analysis of real data. Okumura et al. (2008) concluded that SDSS DR3 LRG data were not sufficient for measuring $H(z)$ and $D_A(z)$; they derived constraints on cosmological parameters assuming that dark energy is a cosmological constant. Cabre & Gaztanaga (2008) measured the linear redshift space distortion parameter β , galaxy bias, and σ_8 from SDSS DR6 LRGs. Gaztanaga, Cabre, & Hui (2009) obtained a measurement of $H(z)$ by measuring the peak of the 2PCF along the line of sight. However, Kazin et al. (2010b) showed that the amplitude of the line-of-sight peak is consistent with sample variance.

In our previous paper, Chuang, Wang, & Hemantha (2012), we presented the method to obtain dark energy and cosmological model constraints from the spherically-averaged 2PCF, without assuming a dark energy model or a flat Universe. We demonstrated the feasibility of extracting $H(z)$ and $D_A(z)$ by scaling the spherically-averaged 2PCF (which leads to highly correlated measurements). In this paper, we obtain robust measurements of $H(z)$ and $D_A(z)$ through scaling, using the 2D correlation function measured from a sample of SDSS DR7 LRGs (Eisenstein et al. 2001). This sample is homogeneous and has the largest effective survey volume to date for studying the quasi-linear regime (Eisenstein et al. 2005). In Section 2, we introduce the galaxy sample used in our study. In Section 3, we describe the details of our method. In Section 4, we present our results. In Section 5, we apply some systematic tests to our measurements. We summarize and conclude in Sec. 6.

2 DATA

The SDSS has observed one-quarter of the entire sky and performed a redshift survey of galaxies, quasars and stars in five passbands u, g, r, i , and z with a 2.5m telescope (Fukugita et al. 1996; Gunn et al. 1998, 2006). We use the public catalog, the NYU Value-Added Galaxy Catalog (VAGC) (Blanton et al. 2005), derived from the SDSS II final public data release, Data Release 7 (DR7) (Abazajian et al. 2009). We select our LRG sample from the NYU VAGC with the flag *primTarget* bit mask set to 32. K-corrections have been applied to the galaxies with a fiducial model (Λ CDM with $\Omega_m = 0.3$ and $h = 1$), and the selected galaxies are required to have rest-frame g -band absolute magnitudes $-23.2 < M_g < -21.2$ (Blanton & Roweis 2007). The same selection criteria were used in previous papers (Zehavi et al. 2005; Eisenstein et al. 2005; Okumura et al. 2008; Kazin et al. 2010a). The sample we use is referred to as “DR7full” in Kazin et al. (2010a). Our sample includes 87000 LRGs in the redshift range 0.16–0.44.¹

Spectra cannot be obtained for objects closer than 55 arcsec within a single spectroscopic tile due to the finite size of the fibers.

¹ We have identified a bug while computing the weighting of each galaxy in the first draft of this paper. The bug was that we computed the weights of random data with the number density of random data instead of observed data. This would introduce a bias when the number density is not homogeneous.

To correct for these “collisions”, the redshift of an object that failed to be measured would be assigned to be the same as the nearest successfully observed one. Both fiber collision corrections and K-corrections have been made in NYU-VAGC (Blanton et al. 2005). The collision corrections applied here are different from what has been suggested in Zehavi et al. (2005). However, the effect should be small since we are using relatively large scale which are less affected by the collision corrections.

We construct the radial selection function as a cubic spline fit to the observed number density histogram with the width $\Delta z = 0.01$. The NYU-VAGC provides the description of the geometry and completeness of the survey in terms of spherical polygons. We adopt it as the angular selection function of our sample. We drop the regions with completeness below 60% to avoid unobserved plates (Zehavi et al. 2005). The Southern Galactic Cap region is also dropped.

3 METHODOLOGY

In this section, we describe the measurement of the correlation function from the observational data, construction of the theoretical prediction, and the likelihood analysis that leads to constraints on dark energy and cosmological parameters.

3.1 Measuring the Two-Dimensional Two-Point Correlation Function

We convert the measured redshifts of galaxies to comoving distances by assuming a fiducial model, Λ CDM with $\Omega_m = 0.25$. We use the two-point correlation function estimator given by Landy & Szalay (1993):

$$\xi(\sigma, \pi) = \frac{DD(\sigma, \pi) - 2DR(\sigma, \pi) + RR(\sigma, \pi)}{RR(\sigma, \pi)}, \quad (1)$$

where π is the separation along the light of sight (LOS), σ is the separation in the plane of the sky, DD, DR, and RR represent the normalized data-data, data-random, and random-random pair counts respectively in a distance range. The LOS is defined as the direction from the observer to the center of a pair. The bin size we use in this study is $10 h^{-1} \text{Mpc} \times 10 h^{-1} \text{Mpc}$. The Landy and Szalay estimator has minimal variance for a Poisson process. Random data are generated with the same radial and angular selection functions as the real data. One can reduce the shot noise due to random data by increasing the number of random data. The number of random data we use is 10 times that of the real data. While calculating the pair counts, we assign to each data point a radial weight of $1/[1 + n(z) \cdot P_w]$, where $n(z)$ is the radial selection function and $P_w = 4 \cdot 10^4 h^{-3} \text{Mpc}^3$ (Eisenstein et al. 2005). We use the same P_w as Eisenstein et al. (2005) in which they used the sample of the SDSS DR3. Although the data release versions are different, the properties of the galaxy sample should be basically the same. We find that the error bars estimated from LasDamas mock catalogs could be improved by 10% while using the weighting (compared to the error bars obtained without using the weighting). We expect that the results should not be sensitive to the P_w used.

3.2 Theoretical Two-Dimensional Two-Point Correlation Function

We compute the linear power spectra at $z = 0.35$ by using CAMB (Lewis, Challinor, & Lasenby 2000). To include the effect

of non-linear structure formation on the BAOs, we first calculate the dewiggled power spectrum

$$P_{dw}(k) = P_{lin}(k) \exp\left(-\frac{k^2}{2k_*^2}\right) + P_{nw}(k) \left[1 - \exp\left(-\frac{k^2}{2k_*^2}\right)\right], \quad (2)$$

where $P_{lin}(k)$ is the linear matter power spectrum, $P_{nw}(k)$ is the no-wiggle or pure CDM power spectrum calculated using Eq.(29) from Eisenstein & Hu (1998), and k_* is marginalized over² with a flat prior over the range of 0.09 to 0.13 $h\text{Mpc}^{-1}$.

We then use the software package *halofit* (Smith et al. 2003) to compute the non-linear matter power spectrum:

$$r_{halofit}(k) \equiv \frac{P_{halofit,nw}(k)}{P_{nw}(k)} \quad (3)$$

$$P_{nl}(k) = P_{dw}(k)r_{halofit}(k), \quad (4)$$

where $P_{halofit,nw}(k)$ is the power spectrum obtained by applying *halofit* to the no-wiggle power spectrum, and $P_{nl}(k)$ is the non-linear power spectrum. We compute the theoretical real space two-point correlation function, $\xi(r)$, by Fourier transforming the non-linear power spectrum $P_{nl}(k)$.

In the linear regime (i.e., large scales) and adopting the small-angle approximation (which is valid on scales of interest), the 2D correlation function in the redshift space can be written as (Kaiser 1987; Hamilton 1992)

$$\xi^*(\sigma, \pi) = \xi_0(s)P_0(\mu) + \xi_2(s)P_2(\mu) + \xi_4(s)P_4(\mu), \quad (5)$$

where $s = \sqrt{\sigma^2 + \pi^2}$, μ is the cosine of the angle between $\mathbf{s} = (\sigma, \pi)$ and the LOS, and P_l are Legendre polynomials. The multipoles of ξ are defined as

$$\xi_0(r) = \left(1 + \frac{2\beta}{3} + \frac{\beta^2}{5}\right) \xi(r), \quad (6)$$

$$\xi_2(r) = \left(\frac{4\beta}{3} + \frac{4\beta^2}{7}\right) [\xi(r) - \bar{\xi}(r)], \quad (7)$$

$$\xi_4(r) = \frac{8\beta^2}{35} \left[\xi(r) + \frac{5}{2}\bar{\xi}(r) - \frac{7}{2}\bar{\bar{\xi}}(r)\right], \quad (8)$$

where β is the redshift space distortion parameter and

$$\bar{\xi}(r) = \frac{3}{r^3} \int_0^r \xi(r') r'^2 dr', \quad (9)$$

$$\bar{\bar{\xi}}(r) = \frac{5}{r^5} \int_0^r \xi(r') r'^4 dr'. \quad (10)$$

Next, we convolve the 2D correlation function with the distribution function of random pairwise velocities, $f(v)$, to obtain the final model $\xi(\sigma, \pi)$ (Peebles 1980)

$$\xi(\sigma, \pi) = \int_{-\infty}^{\infty} \xi^*\left(\sigma, \pi - \frac{v}{H(z)a(z)}\right) f(v) dv, \quad (11)$$

where the random motions are represented by an exponential form (Ratcliffe et al. 1998; Landy 2002)

$$f(v) = \frac{1}{\sigma_v \sqrt{2}} \exp\left(-\frac{\sqrt{2}|v|}{\sigma_v}\right), \quad (12)$$

² Although k_* can be computed by renormalization perturbation theory (Croce & Scoccimarro 2006; Matsubara 2007), doing so requires knowing the amplitude of the power spectrum, which is also marginalized over in this study.

where σ_v is the pairwise peculiar velocity dispersion.

The parameter set we use to compute the theoretical correlation function is $\{H(z), D_A(z), \beta, \Omega_m h^2, \Omega_b h^2, n_s, \sigma_v, k_*\}$, where Ω_m and Ω_b are the density fractions of matter and baryons, n_s is the powerlaw index of the primordial matter power spectrum, and h is the dimensionless Hubble constant ($H_0 = 100h \text{ km s}^{-1} \text{ Mpc}^{-1}$). We set $h = 0.7$ while calculating the non-linear power spectra. On the scales we use for comparison with data, the theoretical correlation function only depends on cosmic curvature and dark energy through parameters $H(z)$ and $D_A(z)$, assuming that dark energy perturbations are unimportant (valid in simplest dark energy models). Thus we are able to extract constraints from data that are independent of a dark energy model and cosmic curvature.

Fig.1(a) shows the 2D 2PCF measured from SDSS LRGs compared with a theoretical model. The measured 2D 2PCF of the SDSS LRGs has been smoothed by a Gaussian filter with rms variance of $2h^{-1} \text{ Mpc}$ to illustrate the comparison of data with model in this figure, as the unsmoothed data are very noisy. Smoothing is *not* used in our likelihood analysis to avoid possibly introducing systematic biases. Fig. 1(b) shows the 2D 2PCF measured from a single LasDamas SDSS LRG mock catalog for comparison. The similarity between the data and the mock in the range of scales we used (indicated by the shaded disk) is apparent.

Fig.2 shows the averaged 2D 2PCF measured from the LasDamas mock catalogs compared with a theoretical model. The contour levels are apparent in the measured 2D 2PCF even though no smoothing is used; this is due to the reduction of shot noise achieved by averaging over 160 mock catalogs. Clearly, our 2D theoretical model provides a reasonable fit to data on intermediate (and quasi-linear) scales. The deviations on smaller scales may be due to the simplicity of the peculiar velocity model we have used. We do not use the smaller scales ($s < 40 h^{-1} \text{ Mpc}$), where the scale dependence of redshift distortion and galaxy bias are not negligible and cannot be accurately determined at present. According to Fig. 5 in Eisenstein et al. (2005) and Fig. 4 in Blake et al. (2011), these effects are negligible at $s > 40 h^{-1} \text{ Mpc}$. On large scales, data become very noisy as sample variance dominates. For these reasons, we will only use the scale range of $s = 40 - 120 h^{-1} \text{ Mpc}$ in our analysis. We do not consider wide-angle effects, since they have been shown to be small on the length scales of interest here (Samushia et al. 2011). Samushia et al. (2011) showed that the corrections (i.e. nonlinear effect and wide-angle effect) to the Kaiser formula are small comparing to the statistical errors on the measurement of the correlation function from SDSS DR7 LRG for the scale range interested ($s=40-120 \text{ Mpc}/h$). In this study, we include the largest correction, dewiggling (nonlinear-BAO), and the nonlinear effects at small scales. Since including a larger range of scales gives more stringent constraints, our choice of $s = 40 - 120 h^{-1} \text{ Mpc}$ represents a conservative cut in data to reduce contamination by systematic uncertainties.

3.3 Covariance Matrix

We use the mock catalogs from the LasDamas simulations³ (McBride et al., in preparation) to estimate the covariance matrix of the observed correlation function. LasDamas provides mock catalogs matching SDSS main galaxy and LRG samples. We use the LRG mock catalogs from the LasDamas gamma release with the

³ <http://lss.phy.vanderbilt.edu/lasdamas/>

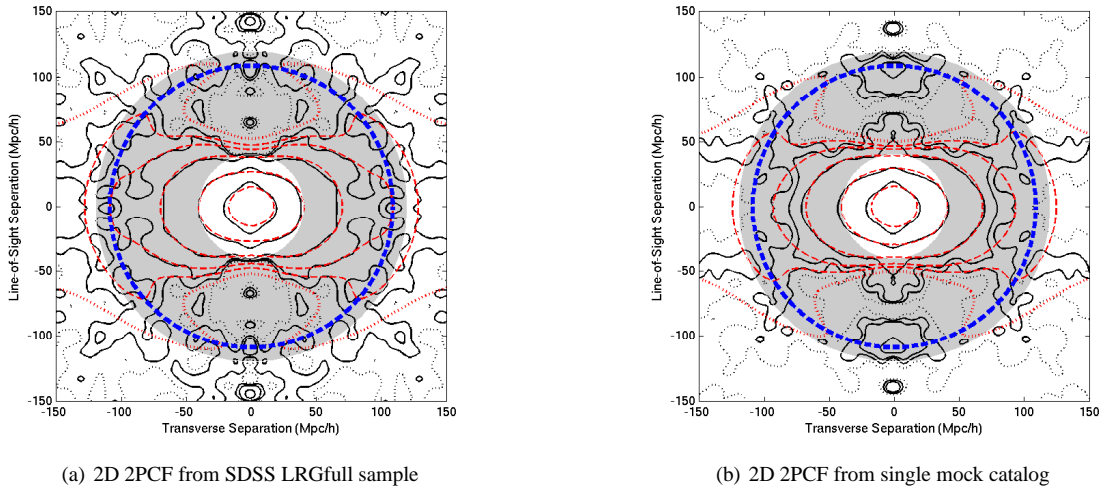


Figure 1. (a) The two-dimensional two-point correlation function (2D 2PCF) measured from SDSS DR7 LRGs in a redshift range $0.16 < z < 0.44$ (solid black contours), compared to a theoretical correlation function with parameters close to the best fit values in the likelihood analysis (dashed red contours). The theoretical model has $H(z = 0.35) = 81.8 \text{ km s}^{-1} \text{ Mpc}^{-1}$, $D_A(z = 0.35) = 1042 \text{ Mpc}$, $\beta = 0.35$, $\Omega_m h^2 = 0.117$, $\Omega_b h^2 = 0.022$, $n_s = 0.96$, $\sigma_v = 300 \text{ km s}^{-1}$, and $k_* = 0.11$. (b) The 2D 2PCF measured from a single mock catalog, compared to a theoretical model with the input parameters of the LasDamas simulations and $\{\beta, \sigma_v, k_*\}$ are set to $\{0.35, 300 \text{ km s}^{-1}, 0.11 h \text{ Mpc}^{-1}\}$ (dashed red contours). In both figures, the shaded disk indicates the scale range considered ($s = 40 - 120 h^{-1} \text{ Mpc}$) in this study. The thick dashed blue circle denotes the baryon acoustic oscillation scale. The observed 2D 2PCF has been smoothed by a Gaussian filter with rms variance of $2h^{-1} \text{ Mpc}$ for illustration in these figures only; smoothing is not used in our likelihood analysis. The contour levels are $\xi = 0.5, 0.1, 0.025, 0.01, 0.005, 0$. The $\xi = 0$ contours are denoted with dotted lines for clarity.

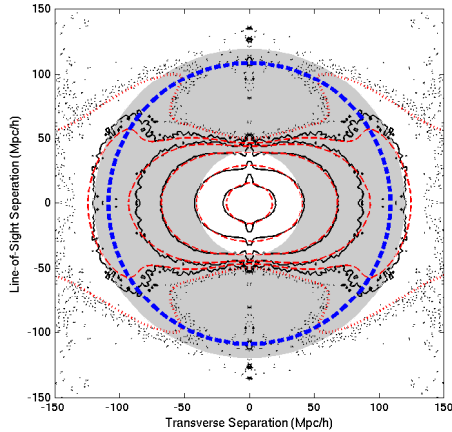


Figure 2. The average two-dimensional two-point correlation function (2D 2PCF) measured from 160 LasDamas SDSS LRGfull mock catalogs (solid black contours), compared to a theoretical model with the input parameters of the LasDamas simulations and $\{\beta, \sigma_v, k_*\}$ are set to $\{0.35, 300 \text{ km s}^{-1}, 0.11 h \text{ Mpc}^{-1}\}$ (dashed red contours). The gray area is the scale range considered ($s = 40 - 120 h^{-1} \text{ Mpc}$) in this study. The thick dashed blue circle denotes the baryon acoustic oscillation scale. The contour levels are apparent in the 2D 2PCF measured from mock catalogs, even though no smoothing is used. The contour levels are $\xi = 0.5, 0.1, 0.025, 0.01, 0.005, 0$. The $\xi = 0$ contours are denoted with dotted lines for clarity.

same cuts as the SDSS LRG DR7full sample, $-23.2 < M_g < -21.2$ and $0.16 < z < 0.44$. We have diluted the mock catalogs to match the radial selection function of the observed data by randomly selecting the mock galaxies according to the number density

of the data sample. We calculate the 2D correlation functions of the mock catalogs and construct the covariance matrix as

$$C_{ij} = \frac{1}{N-1} \sum_{k=1}^N (\bar{\xi}_i - \xi_i^k)(\bar{\xi}_j - \xi_j^k), \quad (13)$$

where N is the number of the mock catalogs, $\bar{\xi}_m$ is the mean of the m^{th} bin of the mock catalog correlation functions, and ξ_m^k is the value in the m^{th} bin of the k^{th} mock catalog correlation function. Note that the covariance matrix constructed from the LasDamas mock catalogs is noisy because only 160 mock catalogs are available. Therefore, we smooth it before using it to calculate the likelihood.

3.4 Likelihood

The likelihood is taken to be proportional to $\exp(-\chi^2/2)$ (Press et al. 1992), with χ^2 given by

$$\chi^2 \equiv \sum_{i,j=1}^{N_{bins}} [\xi_{th}(\mathbf{s}_i) - \xi_{obs}(\mathbf{s}_i)] C_{ij}^{-1} [\xi_{th}(\mathbf{s}_j) - \xi_{obs}(\mathbf{s}_j)] \quad (14)$$

where N_{bins} is the number of bins used, $\mathbf{s}_m = (\sigma_m, \pi_m)$, ξ_{th} is the theoretical correlation function, and ξ_{obs} is the observed correlation function. Note that $\xi_{th}(\mathbf{s}_i)$ depends on $\{H(z), D_A(z), \beta, \Omega_m h^2, \Omega_b h^2, n_s, \sigma_v, k_*\}$.

In principle, we should recalculate the observed correlation function while computing the χ^2 for different models. However, since we don't consider the entire scale range of the correlation function (we only consider $s = 40 - 120 h^{-1} \text{ Mpc}$ in this study), we might include or exclude different data pairs for different models which would render χ^2 values arbitrary. Therefore, instead of recalculating the observed correlation function, we apply the inverse operation to the theoretical correlation function to move the

parameter dependence from the data to the model, thus preserving the number of galaxy pairs used in the likelihood analysis.

Let us define T as the operator converting the measured correlation function from the fiducial model to another model, i.e.,

$$\xi_{obs}(\mathbf{s}) = T(\xi_{obs}^{fid}(\mathbf{s})), \quad (15)$$

where $\xi_{obs}^{fid}(\mathbf{s})$ is the observed correlation function assuming the fiducial model. This allows us to rewrite χ^2 as

$$\chi^2 \equiv \sum_{i,j=1}^{N_{bins}} \{T^{-1}[\xi_{th}(\mathbf{s}_i)] - \xi_{obs}^{fid}(\mathbf{s}_i)\} C_{fid,ij}^{-1} \cdot \{T^{-1}[\xi_{th}(\mathbf{s}_j)] - \xi_{obs}^{fid}(\mathbf{s}_j)\}, \quad (16)$$

where we have used Eqs.(13) and (15).

To find the operator T , note that the fiducial model is only used in converting redshifts into distances for the galaxies in our data sample. In the analysis of galaxy clustering, we only need the separation of a galaxy pair, and not the absolute distances to the galaxies. For a thin redshift shell, the separation of a galaxy pair in the transverse direction is proportional to $D_A(z)\Delta\theta$ ($\Delta\theta$ is the angle separation of the galaxy pair) and the separation along the direction of the line of sight is proportional to $\Delta z/H(z)$ (Δz is the redshift difference between the galaxy pair). Thus, we can convert the separation of one pair of galaxies from the fiducial model to another model by performing the scaling (see, e.g., Seo & Eisenstein (2003))

$$(\sigma', \pi') = \left(\frac{D_A(z)}{D_A^{fid}(z)} \sigma, \frac{H^{fid}(z)}{H(z)} \pi \right). \quad (17)$$

Therefore, we can convert the measured 2D correlation function from some model to the fiducial model as follows:

$$\begin{aligned} \xi_{obs}^{fid}(\sigma, \pi) &= T^{-1}(\xi_{obs}(\sigma, \pi)) \\ &= \xi_{obs} \left(\frac{D_A(z)}{D_A^{fid}(z)} \sigma, \frac{H^{fid}(z)}{H(z)} \pi \right). \end{aligned} \quad (18)$$

This mapping defines the operator T .

We now apply the inverse operation to the theoretical correlation function:

$$T^{-1}(\xi_{th}(\sigma, \pi)) = \xi_{th} \left(\frac{D_A(z)}{D_A^{fid}(z)} \sigma, \frac{H^{fid}(z)}{H(z)} \pi \right). \quad (19)$$

χ^2 can be calculated by substituting eq. (19) into eq. (16).

3.5 Markov Chain Monte-Carlo Likelihood Analysis

We use CosmoMC in a Markov Chain Monte-Carlo likelihood analysis (Lewis & Bridle 2002). The parameter space that we explore spans the parameter set of $\{H(0.35), D_A(0.35), \Omega_m h^2, \beta, \Omega_b h^2, n_s, \sigma_v, k_*\}$. Only $\{H(0.35), D_A(0.35), \Omega_m h^2\}$ are well constrained using SDSS LRGs alone. We marginalize over the other parameters, $\{\beta, \Omega_b h^2, n_s, \sigma_v, k_*\}$, with the flat priors, $\{(0.1, 0.6), (0.01859, 0.02657), (0.865, 1.059), (0, 500) \text{ km s}^{-1}, (0.09, 0.13) h \text{ Mpc}^{-1}\}$, where the flat priors of $\Omega_b h^2$ and n_s are centered on the measurements from WMAP7 and has width of $\pm 7\sigma_{WMAP}$ (with σ_{WMAP} from Komatsu et al. (2010)). These priors are wide enough to ensure that CMB constraints are not double counted when our results are combined with CMB data (Chuang, Wang, & Hemantha 2012). We also marginalize

	mean	σ	lower	upper
$H(0.35)$	82.1	5.0	77.2	86.9
$D_A(0.35)$	1048	58	990	1107
$\Omega_m h^2$	0.118	0.017	0.101	0.133
$H(0.35) r_s(z_d)/c$	0.0434	0.0018	0.0417	0.0451
$D_A(0.35)/r_s(z_d)$	6.60	0.26	6.34	6.85
$D_V(0.35)/r_s(z_d)$	8.62	0.25	8.38	8.86
$A(0.35)$	0.445	0.021	0.425	0.465

Table 1. The mean, standard deviation, and the 68% C.L. bounds of $\{H(0.35), D_A(0.35), \Omega_m h^2, H(0.35) r_s(z_d)/c, D_A(0.35)/r_s(z_d), D_V(0.35)/r_s(z_d), A(0.35)\}$ from SDSS DR7 LRGs. We recommend using $H(0.35) r_s(z_d)/c$ and $D_A(0.35)/r_s(z_d)$ for further analysis. The unit of H is $\text{km s}^{-1} \text{ Mpc}^{-1}$. The unit of D_A, D_V , and $r_s(z_d)$ is Mpc.

over the amplitude of the galaxy correlation function, effectively marginalizing over a linear galaxy bias.

4 RESULTS

We now present the model independent measurements of the parameters $\{H(0.35), D_A(0.35), \Omega_m h^2\}$, obtained by using the method described in previous sections. We also present the derived parameters including $H(0.35) r_s(z_d)/c, D_A(0.35)/r_s(z_d), D_V(0.35)/r_s(z_d)$, and $A(0.35)$, where

$$D_V(z) \equiv \left[(1+z)^2 D_A^2 \frac{cz}{H(z)} \right]^{\frac{1}{3}} \quad (20)$$

and

$$A(z) \equiv D_V(z) \frac{\sqrt{\Omega_m H_0^2}}{cz}. \quad (21)$$

We recommend using $\{H(0.35) r_s(z_d)/c, D_A(0.35)/r_s(z_d)\}$ instead of $\{H(0.35), D_A(0.35), \Omega_m h^2\}$ because they are more robust measurements from this study (see Sec. 5 for more detail). We apply our method to the 2D 2PCF of the LasDamas mock catalogs and find that our measurements are consistent with the input parameters of the simulations.

4.1 Constraints on $H(0.35)$ and $D_A(0.35)$ Independent of a Dark Energy Model

Fig. 3 shows one and two-dimensional marginalized contours of the parameters, $\{H(0.35), D_A(0.35), \Omega_m h^2, H(0.35) r_s(z_d)/c, D_A(0.35)/r_s(z_d), D_V(0.35)/r_s(z_d), A(0.35)\}$, derived in an MCMC likelihood analysis from the measured 2D 2PCF of the SDSS LRG sample. Table 1 lists the mean, rms variance, and 68% confidence level limits of these parameters. Table 2 gives the normalized covariance matrix for this parameter set. These are independent of a dark energy model, and obtained without assuming a flat Universe.

The constraints on $\{H(0.35), D_A(0.35), \Omega_m h^2, H(0.35) r_s(z_d)/c, D_A(0.35)/r_s(z_d), D_V(0.35)/r_s(z_d), A(0.35)\}$, as summarized in Tables 1 and 2, can be used to combined with any other cosmological data set to constrain dark energy and the cosmological model. We recommend using only $\{H(0.35) r_s(z_d)/c, D_A(0.35)/r_s(z_d)\}$ since they have tighter constraints than $\{H(0.35), D_A(0.35)\}$ and are robust in the

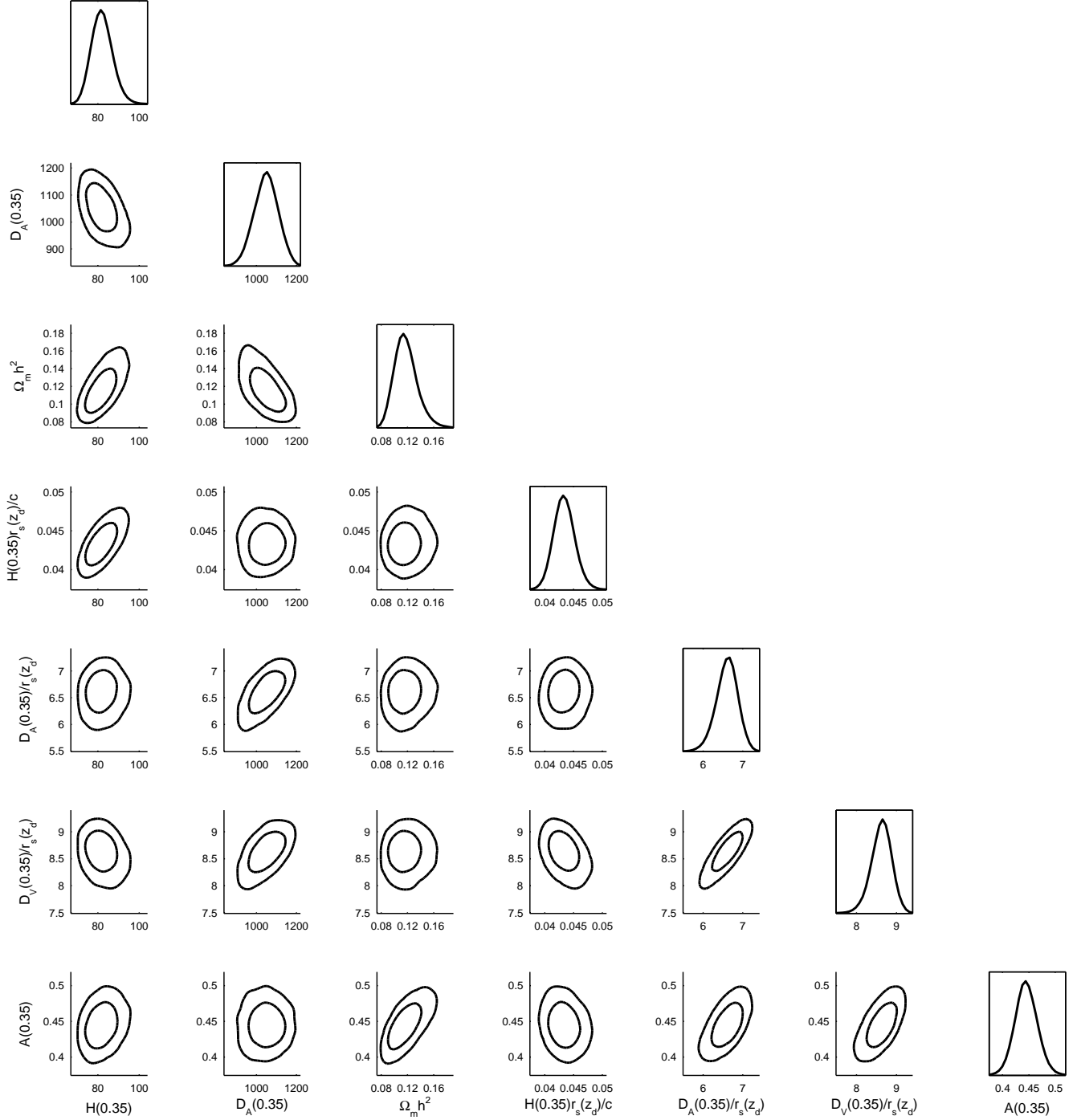


Figure 3. 2D marginalized contours (68% and 95% C.L.) for $\{H(0.35), D_A(0.35), \Omega_m h^2, H(0.35) r_s(z_d)/c, D_A(0.35)/r_s(z_d), D_V(0.35)/r_s(z_d), A(0.35)\}$. The diagonal panels represent the marginalized probabilities. The unit of H is $\text{km s}^{-1} \text{Mpc}^{-1}$. The unit of D_A , D_V , and $r_s(z_d)$ is Mpc.

systematic tests we have carried out (see Sec. 5). In addition, $H(0.35) r_s(z_d)/c$ and $D_A(0.35)/r_s(z_d)$ are basically independent to $\Omega_m h^2$ which might not a robust measurement in this study (see Sec. 5).

The bestfit model from the MCMC likelihood analysis has $\chi^2 = 112$ for 99 bins of data used for a set of 9 parameters (including the overall amplitude of the correlation function) and the χ^2 per degree of freedom ($\chi^2/\text{d.o.f.}$) is 1.24. Note that a

$10 h^{-1} \text{Mpc} \times 10 h^{-1} \text{Mpc}$ bin is used if the center of the bin is in the scale range of $40 h^{-1} \text{Mpc} < s < 120 h^{-1} \text{Mpc}$.

4.2 Validation Using Mock Catalogs

In order to validate our method, we have applied it to 80 2D 2PCFs from 80 LasDamas mock catalogs (which are indexed with 01a-40a and 01b-40b). Again, we apply the flat and wide priors

	$H(0.35)$	$D_A(0.35)$	$\Omega_m h^2$	$H(0.35) r_s(z_d)/c$	$D_A(0.35)/r_s(z_d)$	$D_V(0.35)/r_s(z_d)$	$A(0.35)$
$H(0.35)$	1	-0.4809	0.7088	0.7297	0.0827	-0.2631	0.2618
$D_A(0.35)$	-0.4809	1	-0.6339	-0.0065	0.6730	0.6167	0.0379
$\Omega_m h^2$	0.7088	-0.6339	1	0.0867	0.0888	0.0427	0.7042
$H(0.35) r_s(z_d)/c$	0.7297	-0.0065	0.0867	1	0.0604	-0.4104	-0.1934
$D_A(0.35)/r_s(z_d)$	0.0827	0.6730	0.0888	0.0604	1	0.8851	0.6447
$D_V(0.35)/r_s(z_d)$	-0.2631	0.6167	0.0427	-0.4104	0.8851	1	0.6807
$A(0.35)$	0.2618	0.0379	0.7042	-0.1934	0.6447	0.6807	1

Table 2. Normalized covariance matrix of the measured and derived parameters, $\{H(0.35), D_A(0.35), \Omega_m h^2, H(0.35) r_s(z_d)/c, D_A(0.35)/r_s(z_d), D_V(0.35)/r_s(z_d), A(0.35)\}$.

	mean	σ	input value
$H(0.35)$	81.1	4.1	81.79
$D_A(0.35)$	1009	56	1032.8
$\Omega_m h^2$	0.121	0.013	0.1225
$H(0.35) r_s(z_d)/c$	0.0434	0.0020	0.0434
$D_A(0.35)/r_s(z_d)$	6.26	0.30	6.48
$D_V(0.35)/r_s(z_d)$	8.33	0.31	8.51
$A(0.35)$	0.440	0.019	0.452

Table 3. The mean, standard deviation, and the 68% C.L. bounds of the distributions of the measured values of $\{H(0.35), D_A(0.35), \Omega_m h^2, H(0.35) r_s(z_d)/c, D_A(0.35)/r_s(z_d), D_V(0.35)/r_s(z_d), A(0.35)\}$ from the 2D 2PCF of each of 80 LasDamas mock catalogs (which are indexed with 01a-40a and 01b-40b). Our measurements are consistent with the input values within 1σ , where each σ is computed from the 80 means measured from the 80 mock catalogs. The unit of H is $\text{km s}^{-1} \text{Mpc}^{-1}$. The unit of D_A , D_V , and $r_s(z_d)$ is Mpc.

($\pm 7\sigma_{\text{WMAP7}}$) on $\Omega_b h^2$ and n_s , centered on the input values of the simulation ($\Omega_b h^2 = 0.0196$ and $n_s = 1$).

Table 3 shows the means and standard deviations of the distributions of our measurements of $\{H(0.35), D_A(0.35), \Omega_m h^2, H(0.35) r_s(z_d)/c, D_A(0.35)/r_s(z_d), D_V(0.35)/r_s(z_d), A(0.35)\}$ from each of the LasDamas mock catalogs (80 total) of the SDSS LRG sample. These are consistent with the input parameters, establishing the validity of our method. We also show the measurements of $H(0.35) r_s(z_d)/c$ and $D_A(0.35)/r_s(z_d)$ of each mock catalog in Fig. 4 and Fig. 5. One can see the measurement of $H(0.35) r_s(z_d)/c$ and $D_A(0.35)/r_s(z_d)$ are consistent with the input parameters of the simulations.

4.3 Cross-check with Measurements from Multipoles of the Correlation Function

As a cross-check of our results, we now present the measurements from the monopole-quadrupole of the correlation function for comparison. The detail of the method is described in Appendix B. Table 4 lists the mean, rms variance, and 68% confidence level limits of these parameters. The measurements are consistent with those from our main method (see Table 1). However, the constraints are much weaker ($> 8\%$, which is twice as large as our main results). This is most likely due to the fact that the information used in the monopole-quadrupole method is much less than what we use in our main method (as presented in this paper). It is possible to obtain better measurements using multipole method by including

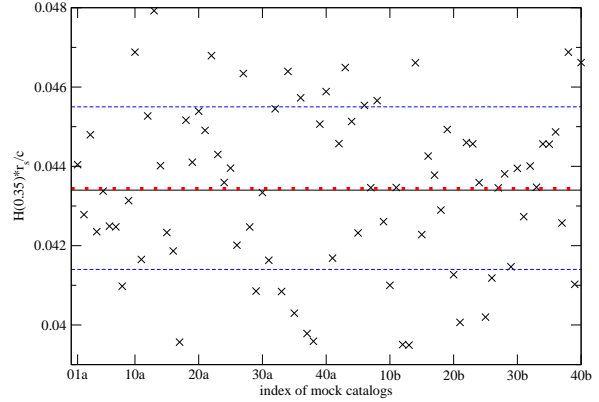


Figure 4. Measurements of the means of $H(0.35) r_s(z_d)/c$ from 80 individual mock catalogs (indexed as 01a to 40a and 01b to 40b). The black solid line shows the mean of these 80 measurements and the blue dashed lines show the range of $\pm\sigma$. The red dotted line shows the theoretical value computed with the input parameters of the simulations.

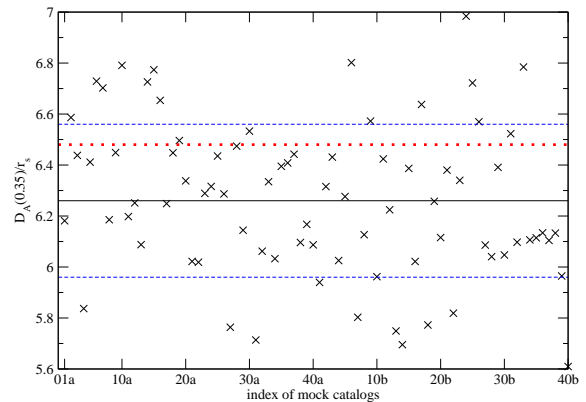


Figure 5. Measurements of the means of $D_A(0.35)/r_s(z_d)$ from 80 individual mock catalogs (indexed as 01a to 40a and 01b to 40b). The black solid line shows the mean of these 80 measurements and the blue dashed lines show the range of $\pm\sigma$. The red dotted line shows the theoretical value computed with the input parameters of the simulations.

	mean	σ	lower	upper
$H(0.35)$	79.6	8.8	70.9	87.8
$D_A(0.35)$	1060	92	970	1150
$\Omega_m h^2$	0.103	0.015	0.088	0.118
$H(0.35) r_s(z_d)/c$	0.0435	0.0045	0.0391	0.0477
$D_A(0.35)/r_s(z_d)$	6.44	0.51	5.99	6.90

Table 4. The mean, standard deviation, and the 68% C.L. bounds of $\{H(0.35), D_A(0.35), \Omega_m h^2, H(0.35) r_s(z_d)/c, D_A(0.35)/r_s(z_d)\}$ from SDSS DR7 LRGs using monopole-quadrupole of the correlation function. The bin size is $5 h^{-1} \text{Mpc}$ and the scale range is $40 < s < 120 h^{-1} \text{Mpc}$. $\chi^2/\text{d.o.f.}$ is 1.23. The unit of H is $\text{km s}^{-1} \text{Mpc}^{-1}$. The unit of D_A , D_V , and $r_s(z_d)$ is Mpc .

higher order multipoles of the correlation function; this is explored in Chuang & Wang (2012).

5 SYSTEMATIC TESTS

Table 5 shows the systematic tests that we have carried out varying key assumptions made in our analysis. These include the range of scales used to calculate the correlation function, the nonlinear damping factor, the bin size, and an overall shift in the measured correlation function due to a systematic error.

First, we fix the nonlinear damping factor, $k_* = 0.11 h \text{Mpc}^{-1}$, and find the results are basically the same. To speed up the computation, we fix k_* for the rest of the tests.

In this study, we marginalize over β with a wide flat prior (0.1 to 0.6) since our method is not sensitive to β . We test fixing the value of β to 0.35, which is close to the measurement from previous work with similar data but using different method (Cabr  & Gaztanaga 2008), and find that our measurements of $H(0.35) r_s(z_d)/c$ and $D_A(0.35)/r_s(z_d)$ change by less than 1% compared to that of marginalizing over β .

We vary the range of the scale and find that $H(0.35) r_s(z_d)/c$ and $D_A(0.35)/r_s(z_d)$ are insensitive to it. However, $\Omega_m h^2$ is sensitive to the minimum scale chosen which could imply that the scale dependent bias or redshift distortion is distorting larger scale than we have expected. Therefore, we do not recommend to use $\Omega_m h^2$ from this study. In the case of $s = 40 - 130 h^{-1} \text{Mpc}$, $D_A(0.35)/r_s(z_d)$ is different from the fiducial result with about 2σ , which is likely due to systematic errors responsible for the anomalously high tail in the spherically-averaged correlation function (see, e.g., Chuang, Wang, & Hemantha (2012)) on large scales.

We vary the bin size to $8 h^{-1} \text{Mpc} \times 8 h^{-1} \text{Mpc}$ and find $\chi^2/\text{d.o.f.} = 1.72$, which can be explained by the increase in the noise level with the increased number of bins. The number of the mock catalogs used to construct the covariance matrix is 160 and the number of bins used with bin size $= 8 h^{-1} \text{Mpc} \times 8 h^{-1} \text{Mpc}$ is 159. One can expect the covariance matrix would be too noisy to give reasonable results.

We also show that the results are insensitive to the constant shift by lowering down the data points of the observed correlation function by 0.001 and 0.002.

6 CONCLUSION AND DISCUSSION

We have obtained the first measurements of $H(z)$ and $D_A(z)$ from galaxy clustering data in an MCMC likeli-

hood analysis. Our constraints for the measured and derived parameters, $\{H(0.35), D_A(0.35), \Omega_m h^2, H(0.35) r_s(z_d)/c, D_A(0.35)/r_s(z_d), D_V(0.35)/r_s(z_d), A(0.35)\}$, from the 2D 2PCF of the sample of SDSS DR7 LRGs are summarized by Tables 1 and 2. Our results are robust and independent of a dark energy model, and obtained without assuming a flat Universe, and represent the first measurements of $H(z)$ and $D_A(z)$ from galaxy clustering data.

Our galaxy clustering measurements of $H(0.35) r_s(z_d)/c$ and $D_A(0.35)/r_s(z_d)$ (see Tables 1 and 2) can be used to combine with CMB and other cosmological data sets to probe dark energy. In a companion paper (Wang, Chuang, & Mukherjee 2012), we explore the implications of our results for dark energy constraints.

We recommend using $H(0.35) r_s(z_d)/c$ and $D_A(0.35)/r_s(z_d)$ measured from the SDSS LRGs for combination with other data sets, since they are tight constraints (4%) that are nearly uncorrelated, and robust with respect to tests of systematic uncertainties. This is as expected, since $H(0.35) r_s(z_d)/c$ and $D_A(0.35)/r_s(z_d)$ correspond to the preferential redshift separation along the line of sight, and the preferential angular separation in the transverse direction respectively; these in turn arise from the BAO in the radial and transverse directions. The measurable preferential redshift and angular separations should be uncorrelated since they are independent degrees of freedom. On the other hand, the measurements of $H(0.35)$ and $D_A(0.35)$ are mainly determined by the geometrical distortion (i.e. the 2D correlation function is supposed to be isotropic without considering the redshift distortion), so that they are highly correlated (correlation coefficient $r \sim -0.5$). The presence of the BAO (although only marginally visible in Fig.1) leads to tight and robust constraints on $H(0.35) r_s(z_d)/c$ and $D_A(0.35)/r_s(z_d)$. Since most of the constraining power in our analysis comes from fitting the overall shape of the galaxy correlation function on quasi-linear scales, and not from fitting the BAO peaks, we refer to our measurements as galaxy clustering measurements.

We have validated our method by applying it to the 2D 2PCF of the mock catalogs from LasDamas, and finding consistency between our measurements and the input parameters of the LasDamas simulations for samples (see Table 3).

As a cross-check of our results, we have measured $H(z)$ and $D_A(z)$ using monopole-quadrupole method and find that the results are consistent with our main method in this study but the constraints are much weaker. The reason is most likely that the information used by the monopole-quadrupole method is much less than what we use in our main method. However, it is still possible to improve the constraints by including higher order multipoles. We explore this issue in Chuang & Wang (2012).

Our work has significant implications for future surveys in establishing the feasibility of measuring both $H(z)$ and $D_A(z)$ from galaxy clustering data. In future work, we will optimize our method, and apply it to new observational data as they become available, and to simulated data of planned surveys to derive robust forecasts for dark energy constraints.

ACKNOWLEDGEMENTS

We would like to thank Chris Blake for useful comments. We are grateful to the LasDamas project for making their mock catalogs publicly available. The computing for this project was performed at the OU Supercomputing Center for Education and Research (OSCER) at the University of Oklahoma (OU). OSCER Director

	$H(0.35)$	$D_A(0.35)$	$\Omega_m h^2$	$\frac{H(0.35)}{c} r_s(z_d)$	$\frac{D_A(0.35)}{r_s(z_d)}$	$\frac{D_V(0.35)}{r_s(z_d)}$	$A(0.35)$	$\chi^2/\text{d.o.f.}$
fiducial result	$82.1^{+4.8}_{-4.9}$	1048^{+59}_{-58}	0.118 ± 0.016	0.0434 ± 0.0017	6.60 ± 0.25	8.62 ± 0.24	0.445 ± 0.020	1.24
$k_* = 0.11$	$81.7^{+4.9}_{-5.0}$	1051 ± 59	$0.116^{+0.016}_{-0.017}$	0.0434 ± 0.0017	6.59 ± 0.25	8.62 ± 0.24	0.443 ± 0.020	1.24
$\beta = 0.35$	83.9 ± 5.6	1008 ± 53	0.132 ± 0.020	$0.0430^{+0.0016}_{-0.0017}$	6.54 ± 0.24	8.60 ± 0.24	0.456 ± 0.021	1.25
$30 < s < 120, k_* = 0.11$	$83.4^{+4.5}_{-4.7}$	1038^{+52}_{-51}	$0.120^{+0.013}_{-0.014}$	$0.0437^{+0.0019}_{-0.0018}$	$6.59^{+0.23}_{-0.22}$	$8.59^{+0.24}_{-0.23}$	0.446 ± 0.016	1.24
$50 < s < 120, k_* = 0.11$	$83.9^{+5.5}_{-5.4}$	1012^{+63}_{-64}	$0.134^{+0.024}_{-0.023}$	0.0428 ± 0.0019	6.59 ± 0.26	$8.65^{+0.24}_{-0.23}$	0.460 ± 0.024	1.06
$40 < s < 110, k_* = 0.11$	80.6 ± 5.1	1087^{+59}_{-60}	0.115 ± 0.016	0.0429 ± 0.0019	$6.78^{+0.27}_{-0.26}$	8.81 ± 0.27	$0.454^{+0.022}_{-0.021}$	1.09
$40 < s < 130, k_* = 0.11$	$84.8^{+6.4}_{-6.3}$	987^{+61}_{-60}	0.115 ± 0.016	0.0451 ± 0.0026	$6.17^{+0.27}_{-0.26}$	8.14 ± 0.28	0.418 ± 0.019	1.31
bin size = $8h^{-1}\text{Mpc} \times 8h^{-1}\text{Mpc}$	$87.9^{+5.6}_{-6.0}$	1037 ± 60	$0.139^{+0.017}_{-0.018}$	$0.0447^{+0.0023}_{-0.0024}$	6.78 ± 0.27	$8.70^{+0.27}_{-0.29}$	$0.470^{+0.021}_{-0.020}$	1.72
shift = $0.001, k_* = 0.11$	$83.0^{+5.4}_{-5.3}$	1041^{+61}_{-60}	$0.124^{+0.019}_{-0.018}$	$0.0433^{+0.0018}_{-0.0018}$	6.63 ± 0.26	$8.65^{+0.25}_{-0.26}$	0.453 ± 0.021	1.25
shift = $0.002, k_* = 0.11$	$85.2^{+5.4}_{-5.6}$	1024^{+63}_{-65}	$0.135^{+0.021}_{-0.020}$	0.0435 ± 0.0019	6.67 ± 0.28	8.67 ± 0.28	0.463 ± 0.022	1.24

Table 5. This table shows the systematic tests with the damping factor, the scale range, the bin size, and the assumed constant shift from a systematic error ($\xi_{obs}(s) = \xi_{true}(s) + \text{shift}$). The fiducial results are obtained by considering the scale range ($40 < s < 120 h^{-1}\text{Mpc}$), the bin size = $10h^{-1}\text{Mpc} \times 10h^{-1}\text{Mpc}$, and the damping factor, k_* , marginalized over with the a flat prior ($0.09 < k_* < 0.13 h\text{Mpc}^{-1}$). The other results are calculated with only specified quantities different from the fiducial one. The unit of H is $\text{km s}^{-1} \text{Mpc}^{-1}$. The unit of D_A , D_V , and $r_s(z_d)$ is Mpc. The unit of k_* is $h\text{Mpc}^{-1}$.

Henry Neeman and HPC Application Software Specialist Joshua Alexander provided invaluable technical support. This work was supported in part by DOE grant DE-FG02-04ER41305.

Funding for the Sloan Digital Sky Survey (SDSS) has been provided by the Alfred P. Sloan Foundation, the Participating Institutions, the National Aeronautics and Space Administration, the National Science Foundation, the U.S. Department of Energy, the Japanese Monbukagakusho, and the Max Planck Society. The SDSS Web site is <http://www.sdss.org/>.

The SDSS is managed by the Astrophysical Research Consortium (ARC) for the Participating Institutions. The Participating Institutions are The University of Chicago, Fermilab, the Institute for Advanced Study, the Japan Participation Group, The Johns Hopkins University, Los Alamos National Laboratory, the Max-Planck-Institute for Astronomy (MPIA), the Max-Planck-Institute for Astrophysics (MPA), New Mexico State University, University of Pittsburgh, Princeton University, the United States Naval Observatory, and the University of Washington.

REFERENCES

- Abazajian, K. N., *et al.* [SDSS Collaboration], *Astrophys. J. Suppl.* **182**, 543 (2009) [arXiv:0812.0649 [astro-ph]].
- Bacon DJ, Refregier AR, Ellis RS *MNRAS* 318:625 (2000)
- Bennett, C. L., *et al.*, *Astrophys. J. Suppl.* **148**, 1 (2003)
- Blake, C., Glazebrook, K, 2003, *ApJ*, 594, 665
- Blake, C.; Collister, A.; Bridle, S.; and Lahav, O., *Mon. Not. Roy. Astron. Soc.* **374**, 1527 (2007) [arXiv:astro-ph/0605303].
- Blake, C., *et al.* 2009, *MNRAS*, 395, 240
- Blake, C.; Davis, T.; Poole, G.; Parkinson, D.; Brough, S.; Colless, M.; Contreras, C.; and Couch, W. *et al.*, *Mon. Not. Roy. Astron. Soc.* **415**, 2892 (2011) [arXiv:1105.2862 [astro-ph.CO]].
- Blanton, M. R., *et al.* [SDSS Collaboration], *Astron. J.* **129**, 2562 (2005) [arXiv:astro-ph/0410166].
- Blanton, M. R.; and Roweis, S., *Astron. J.* **133**, 734 (2007) [arXiv:astro-ph/0606170].
- Cabre, A.; and Gaztanaga, E., *Mon. Not. Roy. Astron. Soc.* **393**, 1183 (2009) [arXiv:0807.2460 [astro-ph]].
- Chuang, C. H.; Wang, Y.; and Hemantha, M. D. P., 2012, *MNRAS*, 423, 1474; arXiv:1008.4822 [astro-ph.CO].
- Chuang, C. H.; and Wang, Y., arXiv:1205.5573 [astro-ph.CO].
- Cimatti, A., *et al.* *Exper. Astron.* **23**, 39 (2009) [arXiv:0804.4433 [astro-ph]].
- Colless, M., *et al.* [The 2DFGRS Collaboration], *Mon. Not. Roy. Astron. Soc.* **328**, 1039 (2001) [arXiv:astro-ph/0106498].
- Colless, M., *et al.*, arXiv:astro-ph/0306581.
- Crocce, M., and Scoccimarro, R., *Phys. Rev. D* **73**, 063520 (2006) [arXiv:astro-ph/0509419].
- Eisenstein, D. J.; and Hu, W., *Astrophys. J.* **496**, 605 (1998) [arXiv:astro-ph/9709112].
- Eisenstein, D. J., *et al.* [SDSS Collaboration], *Astron. J.* **122**, 2267 (2001) [arXiv:astro-ph/0108153].
- Eisenstein, D. J., *et al.* [SDSS Collaboration], *Astrophys. J.* **633**, 560 (2005) [arXiv:astro-ph/0501171].
- Eisenstein, D.J. *et al.* [SDSS Collaboration], *Astron. J.* **142**, 72 (2011) [arXiv:1101.1529 [astro-ph.IM]].
- Fukugita, M.; Ichikawa, T.; Gunn, J. E.; Doi, M.; Shimasaku, K.; and Schneider, D. P., *Astron. J.* **111**, 1748 (1996).
- E. Gaztanaga, A. Cabre and L. Hui, *Mon. Not. Roy. Astron. Soc.* **399**, 1663 (2009) [arXiv:0807.3551 [astro-ph]].
- Gunn, J. E., *et al.* [SDSS Collaboration], *Astron. J.* **116**, 3040 (1998) [arXiv:astro-ph/9809085].
- Gunn, J. E., *et al.* [SDSS Collaboration], *Astron. J.* **131**, 2332 (2006) [arXiv:astro-ph/0602326].
- Hamilton, A. J. S., 1992, *APJL*, 385, L5
- Hutsi, G., arXiv:astro-ph/0507678.
- Kaiser, N., *Mon. Not. Roy. Astron. Soc.* **227**, 1 (1987).
- Kazin, E. A., *et al.*, *Astrophys. J.* **710**, 1444 (2010) [arXiv:0908.2598 [astro-ph.CO]].
- Kazin, E. A.; Blanton, M. R.; Scoccimarro, R.; McBride, C. K.; and Berlind, A. A., *Astrophys. J.* **719**, 1032 (2010) [arXiv:1004.2244 [astro-ph.CO]].
- Kazin, E. A.; Sanchez, A. G.; and Blanton, M. R., *Mon. Not. Roy. Astron. Soc.* **419**, 3223 (2012) [arXiv:1105.2037 [astro-ph.CO]].
- Kaiser N, Wilson G, Luppino GA arXiv:astro-ph/0003338 (2000)
- Komatsu, E., *et al.* [WMAP Collaboration], *Astrophys. J. Suppl.* **192**, 18 (2011) [arXiv:1001.4538 [astro-ph.CO]].
- Landy, S. D.; and Szalay, A. S., *Astrophys. J.* **412**, 64 (1993).
- Landy, S. D., “The Pairwise Velocity Distribution Function of Galaxies in the LCRS, 2dF, *Astrophys. J.* **567**, L1 (2002) [arXiv:astro-ph/0202130].
- Lewis, A.; Challinor, A.; and Lasenby, A., *Astrophys. J.* **538**, 473

- (2000) [arXiv:astro-ph/9911177].
- Lewis, A., and Bridle, S., Phys. Rev. D **66**, 103511 (2002) [arXiv:astro-ph/0205436].
- McBride, C., et al., in preparation
- Martinez, V. J., *et al.*, Astrophys. J. **696**, L93 (2009) [Erratum-ibid. **703**, L184 (2009)] [Astrophys. J. **703**, L184 (2009)] [arXiv:0812.2154 [astro-ph]].
- Matsubara, T., Phys. Rev. D **77**, 063530 (2008) [arXiv:0711.2521 [astro-ph]].
- Okumura, T.; Matsubara, T.; Eisenstein, D. J.; Kayo, I.; Hikage, C.; Szalay, A. S.; and Schneider, D. P., Astrophys. J. **676**, 889 (2008) [arXiv:0711.3640 [astro-ph]].
- Padmanabhan, N., *et al.* [SDSS Collaboration], Mon. Not. Roy. Astron. Soc. **378**, 852 (2007) [arXiv:astro-ph/0605302].
- Padmanabhan, N., and White, M. J., Phys. Rev. D **77**, 123540 (2008) [arXiv:0804.0799 [astro-ph]].
- Peebles, P. J. E. 1980, The Large-Scale Structure of the Universe (Princeton, NJ: Princeton University Press)
- Percival, W. J.; Cole, S.; Eisenstein, D. J.; Nichol, R. C.; Peacock, J. A.; Pope, A. C.; and Szalay, A. S., Mon. Not. Roy. Astron. Soc. **381**, 1053 (2007) [arXiv:0705.3323 [astro-ph]].
- Percival, W. J., *et al.*, Mon. Not. Roy. Astron. Soc. **401**, 2148 (2010) [arXiv:0907.1660 [astro-ph.CO]].
- Perlmutter, S., *et al.* [Supernova Cosmology Project Collaboration], Astrophys. J. **517**, 565 (1999) [arXiv:astro-ph/9812133].
- Press W.H., Teukolsky S.A., Vetterling W.T., Flannery B.P., 1992, Numerical recipes in C. The art of scientific computing, Second edition, Cambridge: The University Press.
- Ratcliffe, A., et al., 1998, VizieR Online Data Catalog, 730, 417
- Reid, B. A., *et al.*, Mon. Not. Roy. Astron. Soc. **404**, 60 (2010) [arXiv:0907.1659 [astro-ph.CO]].
- Riess, A. G., *et al.* [Supernova Search Team Collaboration], Astron. J. **116**, 1009 (1998) [arXiv:astro-ph/9805201].
- Sanchez, A. G.; Crocce, M.; Cabre, A.; Baugh, C. M.; and Gaztanaga, E., Mon. Not. Roy. Astron. Soc. **400**, 3 (2009) [arXiv:0901.2570 [astro-ph]].
- Samushia, L.; Percival, W. J.; and Raccanelli, A., Mon. Not. Roy. Astron. Soc. **420**, 2102 (2012) [arXiv:1102.1014 [astro-ph.CO]].
- Saunders, W., *et al.*, Mon. Not. Roy. Astron. Soc. **317**, 55 (2000) [arXiv:astro-ph/0001117].
- Seo, H., Eisenstein, D. J., 2003, ApJ, 598, 720
- Smith, R. E., *et al.* [The Virgo Consortium Collaboration], Mon. Not. Roy. Astron. Soc. **341**, 1311 (2003) [arXiv:astro-ph/0207664].
- Tegmark, M., *et al.* [SDSS Collaboration], Astrophys. J. **606**, 702 (2004) [arXiv:astro-ph/0310725].
- van Waerbeke, L., et al. *Astron. Astrophys* 358:30 (2000)
- Wang, Y., 2006, ApJ, 647, 1
- Wang, Y., et al., MNRAS, 409, 737 (2010)
- Wang, Y.; Chuang, C. H.; and Mukherjee, P., Phys. Rev. D **85**, 023517 (2012) [arXiv:1109.3172 [astro-ph.CO]].
- Wittman, D. M.; Tyson, J. A.; Kirkmand, D.; Dell’Antonio, I.; Bernstein, G., Nature, 405, 143 (2000)
- Zehavi, I., *et al.* [SDSS Collaboration], Astrophys. J. **621**, 22 (2005) [arXiv:astro-ph/0411557].

APPENDIX A: ALGORITHM OF SMOOTHING THE COVARIANCE MATRIX

The original covariance matrix, C_{ij} , is computed by Eq. (13). Since the correlation function is in two dimension, we could re-label the covariance matrix as a function of the indexes of two bins, $C(\sigma_i, \pi_i, \sigma_j, \pi_j)$. The covariance matrix would be noisy since it is constructed with a small number of the mock catalogs comparing to the number of bins used. One might not obtain converging results while applying MCMC analysis on the observed data or an individual mock catalog, especially considering larger scale range or larger number of bins. We find that smoothing the covariance matrix could solve the problem. We have also checked that the smoothing procedure would not introduce bias by comparing the results from applying the smoothed and the original covariance matrix on the averaged correlation function from 160 mock catalogs. The concept of our smoothing procedure is that the new value of an element of the covariance matrix would be determined by its original value and the values of its neighbor elements. For example, to smooth an array, $f[n]$, we assign the new value at the index, n' , by $\tilde{f}[n'] = (1 - p) \cdot f[n'] + p \cdot (f[n' - 1] + f[n' + 1])/2$ where $0 \leq p \leq 1$. The goal is to make the value be closer to the mean of the neighbors. Notice that while one of the neighbors is not available (i.e. $f[n']$ is the first or last element of the array), we let $f[n']$ be fixed since the mean of the neighbors is not available. The algorithm can be expressed by eq. (A1)

While eq. (A1) can be applied on most of the elements of the covariance matrix, there are some special cases as describle below.

- (1) Diagonal elements: these elements are only determined by the nearby diagonal elements by eq. (A2), since the diagonal elements are supposed to be larger than their off-diagonal neighbors and should not be smoothed using the latter.
- (2) First off-diagonal elements: these elements are only determined by the first off-diagonal elements nearby, i.e. $C(\sigma_i + \Delta s, \pi_i, \sigma_i, \pi_i)$ would be assigned a new value by eq. (A3), since a first off-diagonal element could be very different from its neighboring diagonal elements and should not be smoothed using the latter.

APPENDIX B: MEASURING H AND D_A WITH MULTIPOLES OF THE CORRELATION FUNCTION

Using monopole-quadrupole of power spectrum to break the degeneracy of $H(z)$ and $D_A(z)$ is introduced by Padmanabhan and White (2008). Kazin et al. (2011) tested the method of monopole-quadrupole of correlation function with mock catalogs. The method used in Kazin et al. (2011) is similar but not exactly the same as our method. We describe our method below.

First, we compute the 2D correlation function with bin size, $1 h^{-1} \text{Mpc} \times 1 h^{-1} \text{Mpc}$. Then, we compute the monopole and quadrupole by

$$\xi_0(s) \equiv \frac{\sum_{s - \frac{\Delta s}{2} < \sqrt{\sigma^2 + \pi^2} < s + \frac{\Delta s}{2}} \xi(\sigma, \pi) \sqrt{1 - \mu^2}}{\text{Number of bins used in the numerator}} \quad (\text{B1})$$

and

$$\xi_2(s) \equiv \frac{\sum_{s - \frac{\Delta s}{2} < \sqrt{\sigma^2 + \pi^2} < s + \frac{\Delta s}{2}} \frac{5}{2} \xi(\sigma, \pi) (3\mu^2 - 1) \sqrt{1 - \mu^2}}{\text{Number of bins used in the numerator}}, \quad (\text{B2})$$

where

$$\tilde{C}(\sigma_i, \pi_i, \sigma_j, \pi_j) = (1-p) \cdot C(\sigma_i, \pi_i, \sigma_j, \pi_j) + \frac{p}{m} \cdot \begin{bmatrix} (C(\sigma_i + \Delta s, \pi_i, \sigma_j, \pi_j) + C(\sigma_i - \Delta s, \pi_i, \sigma_j, \pi_j)), \text{ if both elements left are available} \\ (C(\sigma_i, \pi_i + \Delta s, \sigma_j, \pi_j) + C(\sigma_i, \pi_i - \Delta s, \sigma_j, \pi_j)), \text{ if both elements left are available} \\ (C(\sigma_i, \pi_i, \sigma_j + \Delta s, \pi_j) + C(\sigma_i, \pi_i, \sigma_j - \Delta s, \pi_j)), \text{ if both elements left are available} \\ (C(\sigma_i, \pi_i, \sigma_j, \pi_j + \Delta s) + C(\sigma_i, \pi_i, \sigma_j, \pi_j - \Delta s)), \text{ if both elements left are available} \end{bmatrix}, \quad (\text{A1})$$

where m is the number of the neighbor elements used which should be 0, 2, 4, 6, or 8, and Δs is the size of the bin in one direction. We use $p = 0.01$ and $\Delta s = 10 \text{ Mpc/h}$ in this study, but $p = 0$ if $m = 0$. And then, we iterate this procedure for 10 times.

$$\begin{aligned} \tilde{C}(\sigma_i, \pi_i, \sigma_i, \pi_i) &= (1-p) \cdot C(\sigma_i, \pi_i, \sigma_i, \pi_i) \\ &+ \frac{p}{m} \cdot \begin{bmatrix} (C(\sigma_i + \Delta s, \pi_i, \sigma_i + \Delta s, \pi_i) + C(\sigma_i - \Delta s, \pi_i, \sigma_i - \Delta s, \pi_i)), \text{ if both elements left are available} \\ (C(\sigma_i, \pi_i + \Delta s, \sigma_i, \pi_i + \Delta s) + C(\sigma_i, \pi_i - \Delta s, \sigma_i, \pi_i - \Delta s)), \text{ if both elements left are available} \end{bmatrix}, \end{aligned} \quad (\text{A2})$$

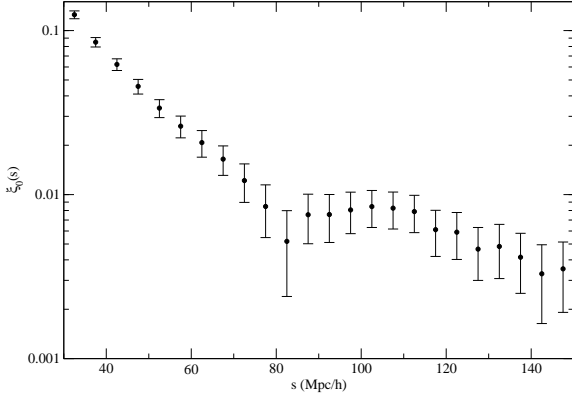


Figure B1. Measurement of monopole of the correlation function from SDSS DR7 LRGs in a redshift range $0.16 < z < 0.44$. The error bars are the square roots of the diagonal elements of the covariance matrix we have derived from mock catalogs.

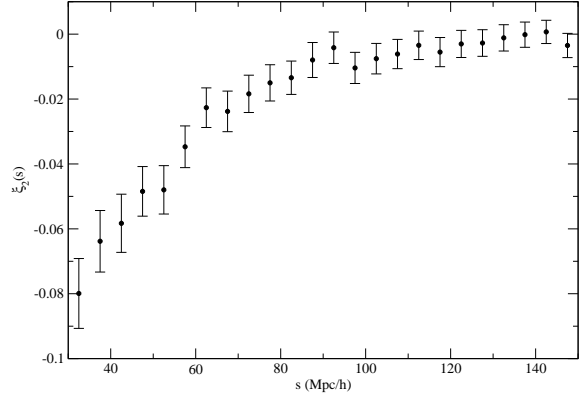


Figure B2. Measurement of quadrupole of the correlation function from SDSS DR7 LRGs in a redshift range $0.16 < z < 0.44$. The error bars are the square roots of the diagonal elements of the covariance matrix we have derived from mock catalogs.

$$\mu \equiv \frac{\pi}{\sqrt{\sigma^2 + \pi^2}} \quad (\text{B3})$$

and $\Delta s = 5 \text{ h}^{-1} \text{Mpc}$ and the scale range used is $40 < s < 120 \text{ h}^{-1} \text{Mpc}$ in this study. Therefore, there are 32 data points for monopole-quadrupole method here, with 16 measurements each for monopole and quadrupole respectively. Fig. B1 and B2 show the measurements of the monopole and quadrupole of the correlation function from the observed galaxy sample.

Just like our main method, the covariance matrix (for the 32 monopole and quadrupole measurements) is constructed from the mock catalogs. The theoretical multipoles are computed using Eqs. (B1) and (B2).

Now, by exploring the same parameters and ranges using MCMC (with χ^2 given by Eq.[16]), one could measure $H(z)$ and $D_A(z)$ following the same steps as our main method in this study. The results are shown in sec. 4.3 (see Table 4). Like our main method, our monopole-quadrupole method has only one approximation, that the observed 2D correlation function using different fiducial models can be converted from one to another with two stretching factors. However, the multipole method tested in Kazin et al. (2011) neglected some additional terms while measuring the stretching factors. Although the effect of the neglected terms might be small, it could be completely avoided by using the method described here.

$$\begin{aligned}
\tilde{C}(\sigma_i + \Delta s, \pi_i, \sigma_i, \pi_i) &= (1 - p) \cdot C(\sigma_i + \Delta s, \pi_i, \sigma_i, \pi_i) \\
&+ \frac{p}{m} \cdot \left[\begin{array}{l} (C(\sigma_i + 2\Delta s, \pi_i, \sigma_i + \Delta s, \pi_j) + C(\sigma_i, \pi_i, \sigma_i - \Delta s, \pi_i)), \text{ if both elements left are available} \\ (C(\sigma_i + \Delta s, \pi_i + \Delta s, \sigma_i, \pi_i + \Delta s) + C(\sigma_i + \Delta s, \pi_i - \Delta s, \sigma_i, \pi_i - \Delta s)), \text{ if both elements left are available} \end{array} \right],
\end{aligned} \tag{A3}$$